Heliyon 9 (2023) e12666

Contents lists available at ScienceDirect

Heliyon

journal homepage: www.cell.com/heliyon

Research article

Xanthine oxidase, a therapeutic target of realgar for non-small cell lung cancer

Rui Guo [a,1], Xiaoyu Gong [b,1], Kongzhao Li [a], Zhengqi Qiu [a], Lina Yang [c], Yanbin Wan [a], Xinhuang Yao [a], Canling Long [a], Jiqing Xu [c], Kang Li [a], Jingyan Liu [d,**], Jia Liu [a,*]

[a] Central Laboratory, The Second Affiliated Hospital, School of Medicine, The Chinese University of Hong Kong, Longgang District People's Hospital of Shenzhen, Shenzhen, Guangdong, 518172, PR China
[b] Pharmacy Department, The Second Affiliated Hospital, School of Medicine, The Chinese University of Hong Kong, Longgang District People's Hospital of Shenzhen, Shenzhen, Guangdong, 518172, PR China
[c] Department of Cardiothoracic Surgery, The Second Affiliated Hospital, School of Medicine, The Chinese University of Hong Kong, Longgang District People's Hospital of Shenzhen, Shenzhen, Guangdong, 518172, PR China
[d] Emergency Department, The Second Affiliated Hospital, School of Medicine, The Chinese University of Hong Kong, Longgang District People's Hospital of Shenzhen, Shenzhen, Guangdong, 518172, PR China

ARTICLE INFO

Keywords:
Molecular docking
Network pharmacology
Realgar
Non-small cell lung cancer
Xanthine oxidase

ABSTRACT

Background: The effects of realgar against non-small cell lung cancer (NSCLC) have been massively studied, but the direct therapeutic targets of realgar remain unclear. This study aimed to identify the molecular targets of realgar against NSCLC and explore their therapeutic mechanisms based on a network pharmacology approach and experimental validations.
Methods: The BATMAN-TCM and Digsee databases were used to predict realgar targets and NSCLC-related genes, respectively. A protein-protein interaction network was constructed for each gene set, and the overlapping genes were identified as potential targets of realgar against NSCLC. The correlation between potential targets and NSCLC was analyzed using The Cancer Genome Atlas and International Cancer Genome Consortium databases, and the key target was validated by in-silico and in-vitro experiments.
Results: Twenty-three overlapping genes, including xanthine oxidase (XO), were identified as potential targets of realgar against NSCLC. XO was selected as the key target for validation, as it was found to be upregulated in NSCLC tumor tissue, which correlated with poor overall survival. A possible interaction between realgar and XO was revealed by molecular docking which was further validated experimentally. Realgar treatment suppressed the activity of XO in NSCLC cells, as demonstrated by the unchanged XO protein levels. Finally, the mechanism of action of XO as a target against NSCLC through the cell-cell junction organization pathway was investigated.
Conclusions: Overall, this study proposes a potential molecular mechanism illustrating that XO is a target of realgar against NSCLC and highlights the usefulness of XO as a therapeutic target for NSCLC.

* Corresponding author. Central Laboratory, The Second Affiliated Hospital, School of Medicine, The Chinese University of Hong Kong, Longgang District People's Hospital of Shenzhen, Shenzhen, Guangdong, 518172, PR China.
** Corresponding author. Emergency Department, The Second Affiliated Hospital, School of Medicine, The Chinese University of Hong Kong, Longgang District People's Hospital of Shenzhen, Shenzhen, Guangdong, 518172, PR China.
E-mail addresses: liujy2597@126.com (J. Liu), liujia870702@126.com (J. Liu).
[1] Equally contributed as first authors.

https://doi.org/10.1016/j.heliyon.2022.e12666
Received 10 July 2022; Received in revised form 18 November 2022; Accepted 20 December 2022
Available online 4 January 2023

1. Introduction

Non-small cell lung cancer (NSCLC) is the leading cause of cancer-related deaths worldwide and accounts for 85% of all lung cancers [1]. Lung adenocarcinoma (LUAD) and lung squamous cell carcinoma (LUSC) are the two main subtypes of NSCLC [2]. Over the past two decades, essential advancements in the treatment of NSCLC have been achieved, increasing our understanding of the disease biology and mechanisms of tumor progression. However, the overall cure and survival benefits of aggressive and metastatic refractory NSCLC remain unsatisfactory [3]. Therefore, continued research on novel targets for treatment and prognosis is required to enhance patient outcomes.

Realgar, a traditional Chinese medicine, has been confirmed to suppress various tumors, including acute promyelocytic leukemia, liver cancer, malignant melanoma, pancreatic cancer, gastric cancer, and cervical cancer [4-10]. Studies have shown that realgar plays an antitumor role by inhibiting the proliferation and migration of tumor cells, suppressing tumor angiogenesis, inducing tumor cell apoptosis, and enhancing antitumor effects [11]. Notably, realgar effectively treats NSCLC along with downregulation of vascular endothelial growth factor (VEGF), hypoxia-inducible factor 1 (HIF-1), basic fibroblast growth factor (b-FGF), and matrix metalloproteinase 9 (MMP-9) [12-14]. Realgar induces apoptosis in A549 cells by inhibiting ribosomal biogenesis proteins and activating the caspases pathway [15]. However, the direct targets of realgar in NSCLC and the underlying mechanisms remain elusive.

In the human body, xanthine oxidase (XO), which is transcribed and translated from the xanthine dehydrogenase (*XDH*) gene, acts as an endogenous enzyme for purine degradation by oxidizing hypoxanthine and xanthine to uric acid [16,17]. During this reaction, XO induces excessive reactive oxygen species (ROS) formation, which is postulated to be important during stages of tumor progression, such as angiogenesis, cell migration, and invasion [18]. Hence, XO inhibition is a potential therapeutic strategy to reduce oxidative stress in cancers [19]. However, the biological significance and role of XO in the pathological processes of NSCLC remain unknown.

In the present study, we aimed to identify the direct targets of realgar in NSCLC and explore their therapeutic mechanisms. The potential mechanisms of action of the realgar against NSCLC were analyzed using network pharmacology. XO was predicted to be a target of realgar against NSCLC. In addition, the *XDH* gene was upregulated in NSCLC tumor tissues, and the elevated expression of *XDH* correlated with poor overall survival in patients with NSCLC. Moreover, realgar treatment decreased XO activity in NSCLC cells but did not change XO protein levels. These findings suggest that XO may be a promising target for the treatment of NSCLC.

2. Material and methods

2.1. Database construction

2.1.1. Prediction of realgar targets

The potential interaction targets of realgar were obtained using BATMAN-TCM (http://bionet.ncpsb.org/batman-tcm/) [20]. BATMAN-TCM is an online bioinformatics analysis tool that is specially used to study the molecular mechanisms and targets of traditional Chinese medicine based on its composition. Prior to target prediction, the international compound identification code (Inchi) of realgar (As_4S_4; 1s/As4S4/c5-1-2-7-3(5)4(6-1)8-2) was acquired from PubChem (http://pubchem.ncbi.nlm.nih.gov). Inchi was input into the BATMAN-TCM tool as a keyword. A cut-off value of more than 2.6 was set to make the prediction more reliable.

2.1.2. Identification of NSCLC-related genes

The DigSee database (http://210.107.182.61/geneSearch/) was used to identify important targets in NSCLC. Digsee is a useful tool to identify the relationship between a "gene" and any "specific disease" by mining the literature through "biological events" such as gene expression, regulation, mutation, localization, phosphorylation, epigenetics, and post-translational modification [21]. The word "Lung Neoplasms" from the system was selected and input into the DigSee database as a keyword. Biological events included mutation, gene expression, regulation, protein catabolism, phosphorylation, localization, binding, transcription, hydroxylation, ubiquitination, DNA methylation, glycosylation, acetylation, methylation, and catalysis. To enhance accuracy, we set the cut-off value for the number of papers as 2, that is, the genes that have been reported to be associated with NSCLC in at least two papers were searched for.

2.2. Bioinformatics analysis

2.2.1. Protein-protein interaction (PPI) network construction

PPI data were obtained from the STRING database (https://string-db.org/, version 10.5), a search tool that could predict interactions among known proteins, thereby facilitating the scientific interpretation of multiple relationships between proteins [22]. The Cytoscape software (https://cytoscape.org/, version 3.7.2) was used to visualize the networks. In the graphs, genes or proteins are indicated by nodes and the interactions are encoded by edges. The Cytoscape plug-in molecule Cytohubba was used to analyze the correlation between realgar targets and NSCLC-related genes.

2.2.2. Acquisition of realgar targets against NSCLC

Venn diagrams (http://bioinformatics.psb.ugent.be/webtools/Venn/) were used to calculate the intersection of a list of realgar targets and NSCLC-related genes [23]. The overlapping genes obtained were considered potential targets of realgar against NSCLC.

2.2.3. Gene ontology (GO) enrichment analysis

GO enrichment analysis of target genes was performed using the Database for Annotation, Visualization, and Integrated Discovery (DAVID version 6.8, https://david.ncifcrf.gov/) to retrieve information regarding the functional annotation of genes [24]. All three aspects: biological process (BP), molecular function (MF) and cellular component (CC), were included in the GO enrichment analysis. GO enrichment analysis results were selected with a p-value of less than 0.05.

2.2.4. Gene expression analysis and survival analysis

RNA-Seq expression and clinical data for patients with NSCLC were obtained from The Cancer Genome Atlas (TCGA) database (http://cancergenome.nih.gov/). LUAD and LUSC datasets were obtained from TCGA. Gene expression and overall survival analyses of *XDH* were performed using GEPIA (http://gepia.cancer-pku.cn/) [25]. Violin plots and pairwise boxplots were used to visualize the differences in *XDH* expression between the tumor and cancer-adjacent tissues for discrete variables. Differences in overall survival between "high" and "low" expression groups (defined by the median value of *XDH* expression) were compared using Kaplan-Meier curves, with *p*-values calculated via log-rank test.

2.2.5. Immunohistochemistry (IHC) analysis

To estimate XO expression at the protein level, IHC images of XO protein expression in normal and lung tumor tissues were downloaded from the Human Protein Atlas database (http://www.proteinatlas.org/).

2.2.6. Pan-cancer analysis of TCGA dataset

The pan-cancer gene expression and patient annotation datasets from TCGA were retrieved from the Genomic Data Commons (GDC) of the National Cancer Institute. Sample-wise gene set activities of different pathways were calculated in Gene Set Variation Analysis (GSVA) using the "ssGSEA" method, and signature scores of different types of immune cells were calculated in GSVA using the "z-score" method. Spearman's correlation and multiple testing corrections were performed using R 4.0.5. Gene Set Enrichment Analysis (GSEA) was performed using the GSEA v4.0 desktop application.

2.2.7. Pathway analysis

The Pearson and Spearman correlation coefficients were used to screen the top 500 differentially expressed genes related to *XDH* expression. These 500 genes were then introduced into FUNRICH analysis software (http://www.funrich.org/) to enrich the pathways [26]. GSEA was conducted on patients with NSCLC and low or high *XDH* expression. The most significantly enriched signaling pathways were selected based on their normalized enrichment scores (NES).

2.2.8. Molecular docking

Molecular docking is an *in silico* target prediction tool that has been widely used to evaluate the preferred binding conformation of small molecules to proteins based on their structures. The three-dimensional structure of XO was downloaded from the Protein Data Bank (PDB) database (http://www.rcsb.org). The chemical structure of realgar was obtained from the PubChem database (https://pubchem.ncbi.nlm.nih.gov/). Before docking, the co-crystallized ligands and water molecules were removed and the hydrogen atoms were affixed from XO. Docking simulations were performed using AutoDockTools (http://mgltools.scripps.edu/, version 1.5.6) [27]. The docking operation process was strictly performed as described in the software instruction manual. To cover all residues with a grid map, each grid point in the x-, y-, and z-axes was set to 126 × 126 × 126 with X = 58.771, Y = 1.284, and Z = 35.96. The remaining parameters were set to default values. The PyMOL software (https://pymol.org/2/, version 2.2) was used to visualize the 3D structure of the docking results.

2.3. Cellular experiments

BEAS-2B, A549 and MES-1 cell lines were purchased from Shanghai Genechem Co., Ltd.

2.3.1. XO activity assay

XO activity was determined using an XO enzyme activity assay kit (A002-1-1, Nanjing Jiancheng Bioengineering Institute) according to the manufacturer's instructions. Briefly, detached A549 cells were treated with reagents 1–4 and incubated at 37 °C for 20 min. After the addition of reagent 5, the absorbance of the sample was measured at 530 nm using a 96-well plate reader.

2.3.2. Cell viability

Cell growth was assessed using the CCK8 assay. Briefly, A549 cells (1×10^3 cells/well) were seeded into 96-well plates. The next day, the cells were treated with 20, 60, and 100 μg/mL of realgar. After 48 h, 10 μL of CCK8 solution was added to each well and incubated for 1 h before absorbance was measured at 450 nm.

2.3.3. Western blotting

Western blotting was performed as described previously [28] with primary antibodies directed against XO (1:1000; Protein Tech; catalog number: 55156-1-AP), E-cadherin (1:500; GENXSPAN, catalog number: GXP94745), ZO-1 (1:1000; Invitrogen, catalog number: 33-9100), glyceraldehyde 3-phosphate dehydrogenase (GAPDH; loading control; 1:5000; Protein Tech; catalog number: 10494-1-AP) and goat anti-rabbit IgG secondary antibodies linked to horseradish peroxidase (1:5000; Protein Tech; catalog number:

SA00001-2). Data were analyzed using ImageJ with GAPDH signals as an internal control.

2.4. Statistical analysis

Data are presented as mean ± standard deviation (SD). The activity and expression levels of XO were analyzed using the Student's *t*-test. GraphPad Prism 8.0 was used for the calculations. Differences were considered statistically significant at $p < 0.05$. Other analyses were conducted using the R software (v.4.0.5). The cut-off value for *XDH* expression was determined using the median value.

3. Results

3.1. Realgar target prediction and network construction

Tetra-arsenic tetra-sulfide (α-As_4S_4) [29] is the primary component of realgar, accounting for more than 90% of the realgar components. To investigate the targets of realgar, target prediction was conducted based on the BATMAN-TCM database, using the

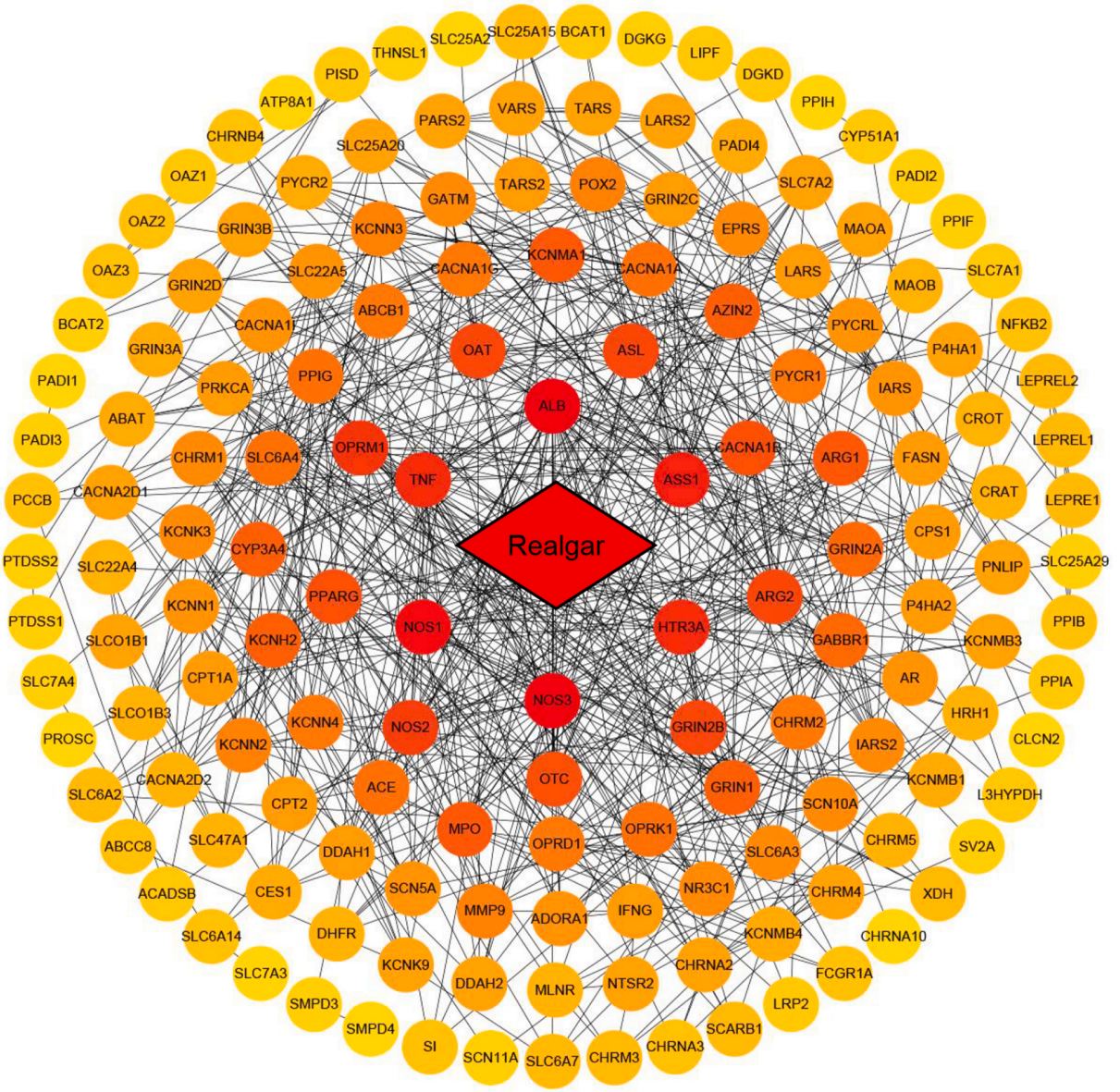

Fig. 1. The network of realgar targets. The red diamond represents realgar. The circles represent the realgar target genes. Nodes are presented in colors varying from yellow to red in increasing order of interaction scores.

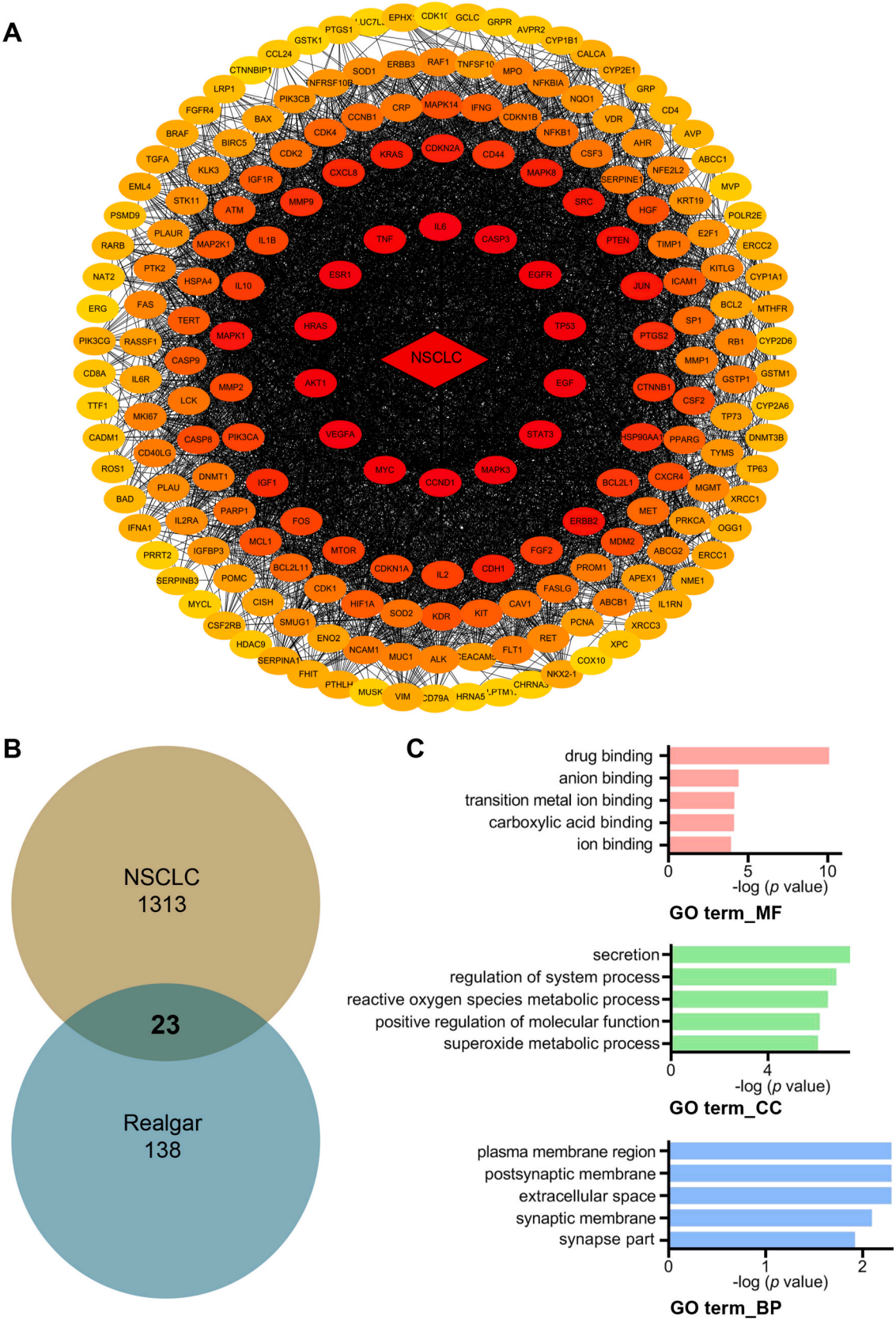

(caption on next page)

Fig. 2. Targets of realgar against NSCLC. (A) The network of NSCLC-related genes. The ellipses represent NSCLC-related genes. Nodes are presented in colors varying from yellow to red in increasing order of interaction scores. (B) Venn diagram reveals overlapping target genes for NSCLC and realgar. (C) Analyses of targets by GO enrichment. The order of importance was ranked by −Log 10 (*p*-value) with a bar chart. NSCLC, non-small cell lung cancer; GO: gene ontology; BP, biological process; MF, molecular function; CC, cellular component.

Inchi of As_4S_4 as the keyword input. In total, 161 realgar targets were obtained, with a cut-off value of 2.6. The PPI network was constructed and visualized using the STRING database and Cytoscape software to clarify the relationships between these targets. According to the network, there were 156 nodes and 680 edges, of which albumin (*ALB*), nitric oxide synthase 1 (*NOS1*), nitric oxide synthase 3 (*NOS3*), tumor necrosis factor (*TNF*), and argininosuccinate synthase 1 (*ASS1*) were hub targets, suggesting that they could

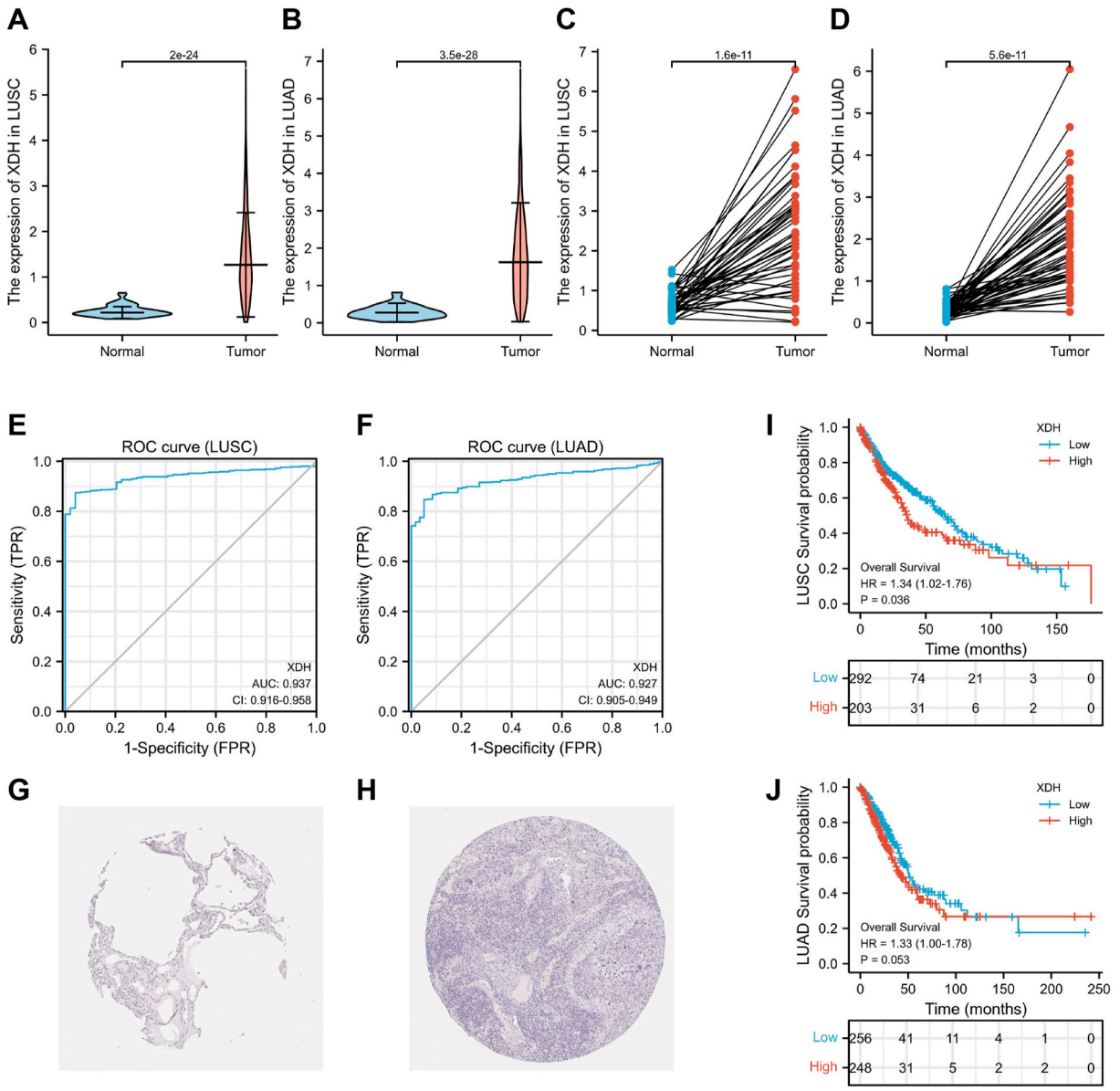

Fig. 3. *XDH* expression level was positively correlated with NSCLC. (A and B) *XDH* expression was significantly upregulated in LUAD (A, n = 49 for Normal; n = 502 for Tumor) and LUSC (B, n = 59 for Normal; n = 535 for Tumor) tissues compared to the para-carcinoma tissue. (C and D) Pairwise boxplots showed differential expression levels of *XDH* in LUSC (C, n = 49) and LUAD (D, n = 59) tissues paired to their para-carcinoma tissues. (E and F) The areas under the ROC curves were 0.937 (95% CI: 0.916–0.958) and 0.927 (95% CI: 0.905–0.949) for LUSC (E) and LUAD (F), respectively. (G and H) XO was upregulated in NSCLC tissue (H) compared to para-carcinoma tissue (G) as indicated by the immunohistochemical image from The Human Protein Atlas database. (I and J) High *XDH* expression is associated with poor survival in patients with LUAD (I) and LUSC (J). LUAD, lung adenocarcinoma; LUSC, lung squamous cell carcinoma. ROC:Receiver Operating Characteristic Curve.

be the primary targets for realgar treatment of the disease (Fig. 1).

3.2. Network diagram of lung cancer-related genes

The Digsee database was used to identify the genes associated with lung cancer. A total of 1337 genes have been reported to be associated with lung cancer in two or more studies. Similarly, a PPI network was constructed to represent the relationships between these genes. The network contained 1293 nodes and 46,879 edges, in which the top 200 related genes with 196 nodes and 4898 edges are shown in Fig. 2A. Among these, *TNF,* interleukin-6 (*IL-6*), caspase 3 (*CASP3*), epidermal growth factor receptor (*EGFR*), tumor protein 53 (*TP53*), epidermal growth factor (*EGF*), signal transducer and activator of transcription 3 (*STAT3*), mitogen-activated protein kinase 3 (*MAPK3*), cyclinD1 (*CCND1*), MYC proto-oncogene *(MYC)*, vascular endothelial growth factor A (*VEGFA*), AKT serine/threonine kinase 1 (*AKT1*), HRas proto-oncogene (*HRAS*), and estrogen receptor 1 (*ESR1*) were the central genes in this network and possessed the most edges.

3.3. Targets of realgar against NSCLC and GO enrichment analysis

Twenty-three overlapping genes were identified as potential targets of realgar against NSCLC (Fig. 2B, Supplementary Table 1). Additionally, these targets were further analyzed using DAVID bioinformatics resources for GO term enrichment analysis to reveal the possible mechanisms involved in realgar for NSCLC treatment. The top five enriched terms based on the *p*-value were obtained from identified targets at three levels: BP, MF, and CC. The results indicated that realgar acted on NSCLC cells through drug binding, secretion, regulation of system processes, reactive oxygen species metabolic processes, positive regulation of molecular functions, and superoxide metabolic processes (Fig. 2C).

3.4. Differential expression and prognostic value of targets between NSCLC and normal tissue samples

Realgar may mediate its antitumor role by inhibiting the activity of targets that are upregulated in cancer tissues and are associated with poor prognosis in patients with cancer. Alternatively, realgar may activate the activity of downregulated targets expressed in cancer tissues, whose low expression is associated with poor prognosis. Therefore, differential gene expression and survival analysis of these targets were performed on the dataset of LUAD and LUSC from the TCGA database to further filter the key targets of realgar. *DHFR, MMP9*, and *XDH* were highly expressed in both LUAD and LUSC tissues than in their para-carcinoma counterparts (Supplementary Figs. 1–3, Fig. 3A and B). *ACE, ALB, CHRM1, MPO*, and *NOS3* expression levels were significantly lower in both LUAD and

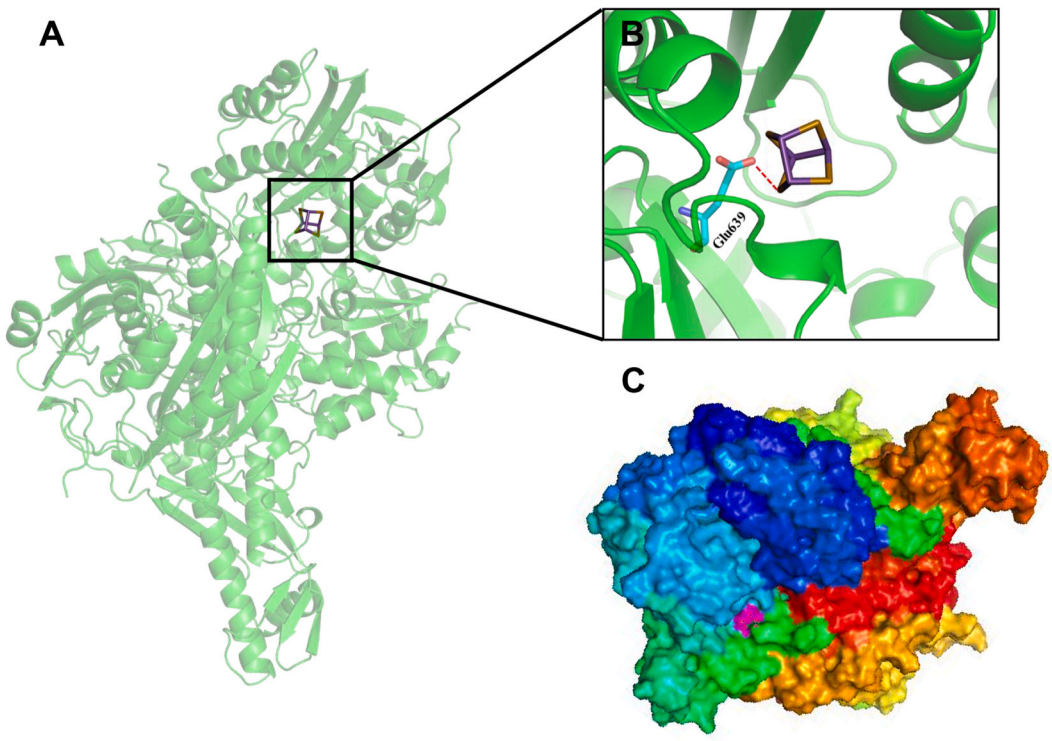

Fig. 4. Molecular docking simulation of realgar to XO. (A and B) Specific binding site of XO and realgar. (C) The purple surface represents the 3D structure of realgar. The polychrome surface represents the protein structure of XO.

LUSC tissues than in the corresponding para-carcinoma tissues (Supplementary Figs. 1–3). We further studied the correlation between the target expression levels and patient prognosis. Only *XDH* was differentially expressed in NSCLC, and its differential expression was positively correlated with poor prognosis (Supplementary Figs. 1–3, Fig. 3I and J). Hence, *XDH* was chosen as the key target of realgar against NSCLC.

Subsequently, paired analysis was performed to further confirm the upregulation of *XDH* expression in LUSC and LUAD compared to their expression in paired para-carcinoma tissues (Fig. 3C and D). These results were highly sensitive and specific, as demonstrated by the Receiver Operating Characteristic Curve (ROC) analysis (Fig. 3E and F). Furthermore, to evaluate XO expression at the protein level, we analyzed IHC results provided by the HPA database and compared the results to XO gene expression data from TCGA. As shown in Fig. 3G and H, XO staining was weak in normal lung tissue but strong in tumor tissue. The protein expression level of XO was relatively high in NSCLC tissue, consistent with the results of TCGA data analysis. Survival analysis indicated that elevated expression of *XDH* was associated with poor overall survival in patients with LUSC, as evaluated by Kaplan–Meier curves (Fig. 3I). Similarly, patients with high levels of *XDH* expression in LUAD displayed a tendency for unfavorable overall survival, although this was not statistically significant (Fig. 3J; $p = 0.053$). Overall, these results indicated that *XDH* could be of value in distinguishing between NSCLC tissue and para-cancer tissue and played a vital role in the survival of patients with NSCLC, suggesting that realgar could act on XO to improve the prognosis of patients.

3.5. Molecular docking analysis of realgar and XO

To better understand the interaction between realgar and XO, molecular docking was applied to evaluate the binding sites using AutoDock Tools. By retrieving the binding affinities of realgar and XO, we identified the most potent binding site with a binding energy of −5.12 kcal/mol, a ligand efficiency of −0.64, and an inhibitor constant of 176.83 μm. In addition, realgar was found to interact with the XO amino acid Glu639 via hydrogen bonding. As shown in the figures, realgar formed a hydrogen bond with Glu639 of XO and also constituted hydrophobic interactions with a series of residues within the binding pocket (Fig. 4A–C). Together, these results indicate a

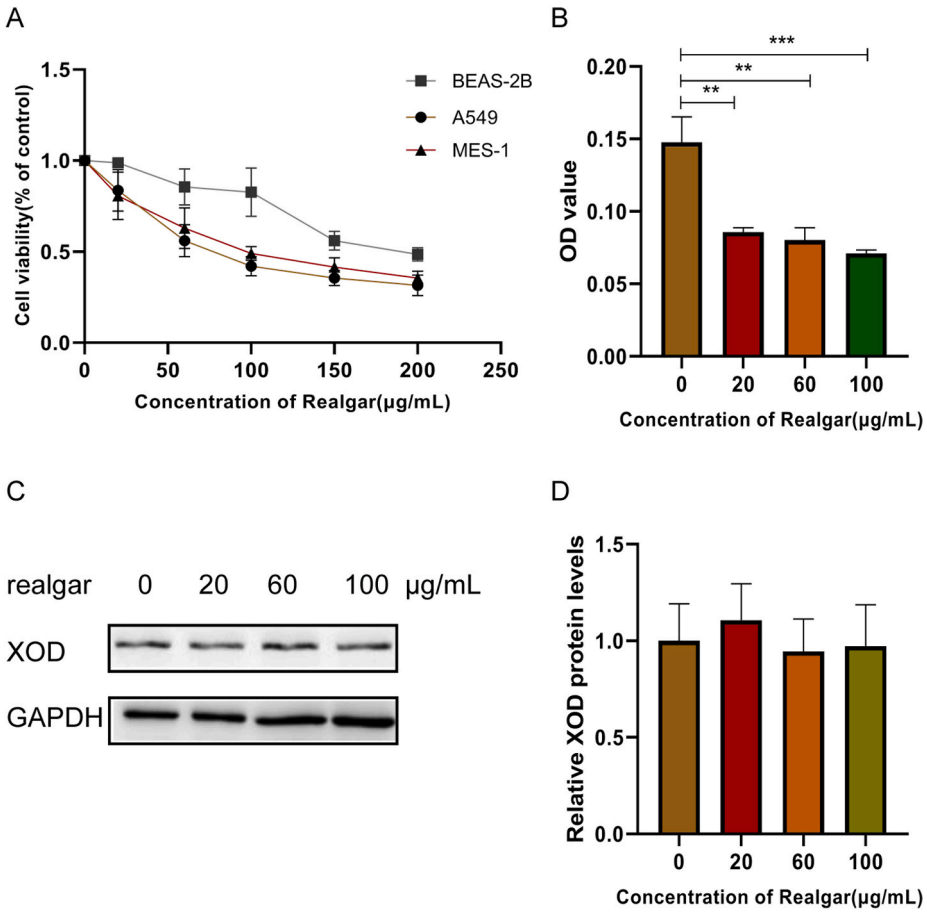

Fig. 5. Inhibition of XO activity by realgar in NSCLC. (A) Cytotoxicity of reaglar in BEAS-2B, A549 and MES-1 cells indicated by the CCK8 assay. (B) XO activity significantly decreased in the treatment with realgar. (C and D) XO protein level was not affected by realgar treatment. The non-adjusted images were shown in Supplementary Fig. 4.

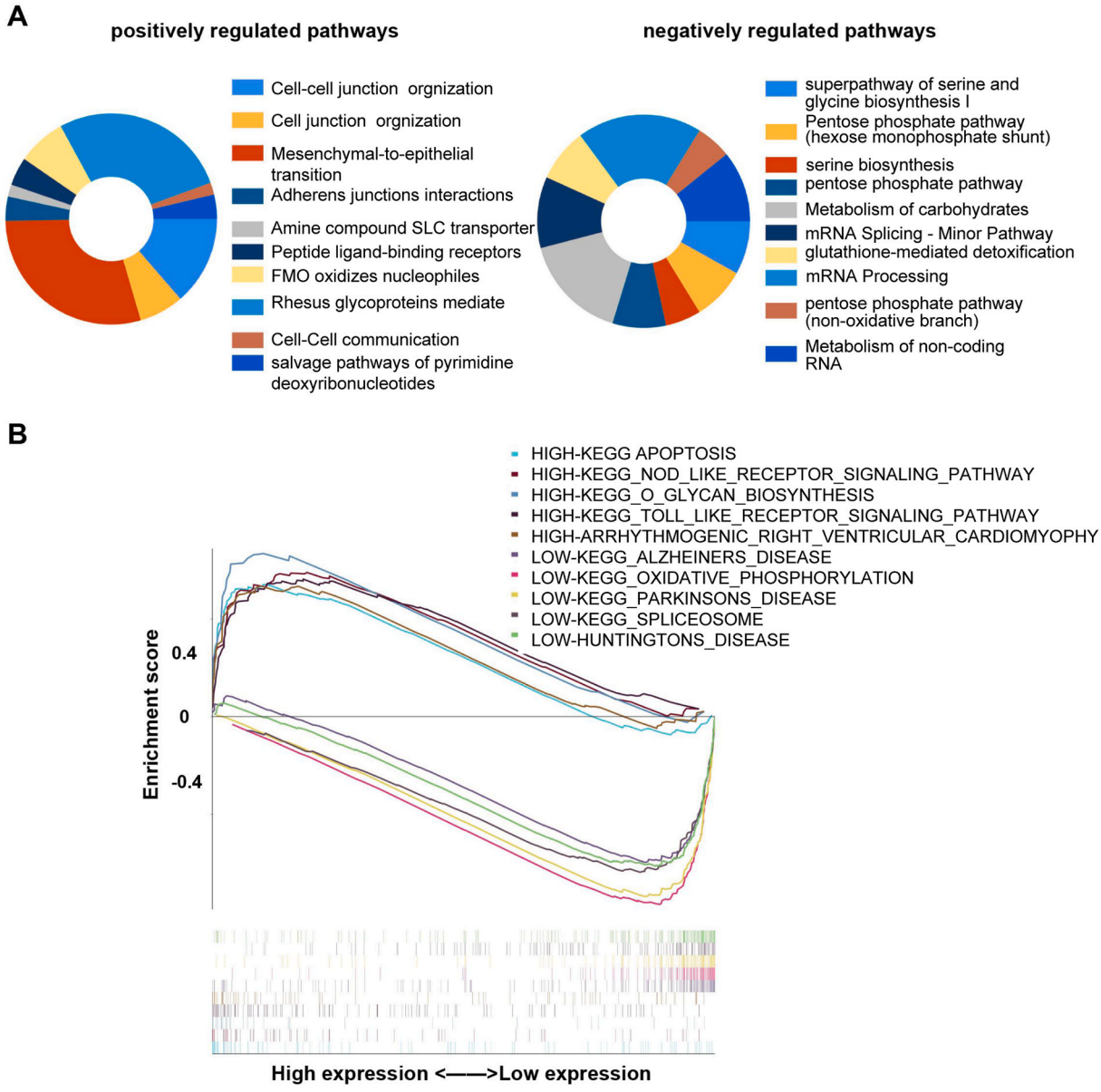

(caption on next page)

Fig. 6. Pathway enrichment analysis of *XDH* co-expressed genes. (A) Biological pathway enrichment analysis of the target genes was performed using FunRich. (B) Pathways analyzed using GESA were shown to be significant in enrichment scores concerning high expression versus low expression of the *XDH* gene. (C and D) ZO-1 and E-cadenrin protein levels in A549 cells upon realgar treatment were detected by Western blot. The non-adjusted images were shown in Supplementary Fig. 5.

direct binding potential between realgar and XO.

3.6. Validation of XO activity inhibition by realgar

To further validate the realgar amelioration of NSCLC by targeting XO, an *in vitro* study was conducted. First, 1 normal human lung epithelial cell line (BEAS-2B) and 2 NSCLC cell lines (A549 and MES-1) were used to evaluate the cytotoxicity of realgar. Cells were treated with different concentrations of realgar (0, 20, 60, 100, 150 and 200 μg/mL) for 24 h. Following treatment, cell viability was decreased along with the increased dosage of realgar. The half inhibitory concentration (IC50) values for BEAS-2B, A549 and MES-1 were 208.12, 79.68 and 108.57 μg/mL, respectively (Fig. 5A). The results indicated that the NSCLC cell lines were more sensitive to realgar than the normal lung cells. Besides, the cell viability was suppressed by realgar dose-dependently.

Next, an XO activity assay was performed to investigate whether the antitumor effect of realgar acted by inhibiting the activity of XO in A549 cells. As shown in Fig. 5B–D and Supplementary Fig. 4, XO activity significantly decreased as the concentration of realgar increased, while the expression level of XO did not change. These data indicated that realgar suppressed NSCLC and inhibited XO activity.

3.7. Possible mechanisms of XO as NSCLC target

To explore the biological significance of XO expression in NSCLC, we performed FunRich analysis of the differentially expressed genes associated with XO expression in NSCLC. The results of the pathway analysis demonstrated that XO positively regulated Cell-cell junction orgnization, cell junction orgnization mesenchymal to epithelial transition (EMT), adherens junctions interactions, peptide ligand-binding receptors, FMO oxidizes nucleophiles (Fig. 6A). In contrast, XO was predicted to be a negative regulator of mRNA processing, carbohydrate metabolism, and metabolism of non-coding RNA pathways (Fig. 6A).

We conducted GSEA to investigate the biological significance of XO expression in NSCLC. The top five pathways significantly positively and negatively associated with XO expression in NSCLC are shown in Fig. 6B. These data indicate that XO expression is positively correlated with the toll-like receptor and the glycan biosynthesis nod-like receptor signaling pathways. In contrast, XO expression was negatively associated with pathways linked to oxidative phosphorylation, Parkinson's disease, and spliceosome (Fig. 6B). These data suggest the possible mechanisms of action of *XDH* as a therapeutic target for NSCLC.

Based on the pathway analysis, realgar is predicted to inhibit the viability of NSCLC cells by regulating the cell-cell junction organization pathway. Subsequently, the expression of classical tight junction (ZO-1) and cadherin (E-cadherin) in A549 cells upon realgar treatment was detected to investigate the mechanism of realgar against NSCLC. Both ZO-1 and E-cadherin protein levels were upregulated with the treatment of the increased realgar concentration (Fig. 6C and D and Supplementary Fig. 5). Overall, the results indicated that realgar reduced the activity of XO and functioned on the cell-cell junction organization pathway, therefore exerting anti-NSCLC effects.

4. Discussion

Recently, network pharmacology has been proven to be a platform for evaluating the molecular mechanisms of drugs from a multidimensional perspective [30,31]. In this study, we investigated the potential molecular mechanisms of action of realgar against NSCLC. By combining network pharmacology, molecular docking, and cellular experiments, we predicted that XO was a promising target of realgar against NSCLC.

Through analysis of a bioinformatics prediction database, we screened 161 putative targets of realgar. The PPI network showed strong interactions within the realgar targets, suggesting the complexity of the mechanisms involved in realgar biological functions. NSCLC-related genes were identified based on the published literature. A total of 1371 genes were selected, with the requirement that they were reported at least twice to enhance accuracy. By considering the overlapping genes between the two lists, 23 genes were identified as realgar targets against NSCLC. According to the GO enrichment analysis, these targets were enriched in drug binding, secretion, regulation of system processes, reactive oxygen species metabolic processes, positive regulation of molecular functions, and superoxide metabolic processes. This result indicates that realgar may have multiple functional roles in the treatment of NSCLC.

Next, we found that *XDH* was the only one of the 23 potential targets that were differentially expressed in both LUAD and LUSC tumor tissues, and the expression level was positively correlated with prognosis. *XDH* was highly expressed in both LUAD and LUSC tumor tissues, and elevated expression of *XDH* was associated with poor survival of patients with LUAD or LUSC. Studies have reported that XO can induce autophagy in NSCLC cells, and inhibition of autophagy in NSCLC cells reduces their proliferation and migration ability [32]. These results suggest that realgar may suppress autophagy by inhibiting XO activity, disrupting autophagy-mediated energy homeostasis, and affecting tumor activity. Results from the network analysis also revealed that alterations in XO expression in the NSCLC phenotype were involved in the cell-cell junction organization, cell junction organization, EMT, adherens junction interactions, peptide ligand-binding receptors, FMO oxidizes nucleophiles.

Cell-cell junction organization pathway was predicted as a potential mechanism of realgar against NSCLC. Cell-cell junctions, including the tight junction, adherens junction and desmosomes, play an important role in regulating cell proliferation. ZO-1 and E-cadherin are the classical tight junction and cadherin, respectively, which were detected in A549 cells at protein levels. Upon the increased concentration of realgar treatment, ZO-1 and E-cadherin expression were upregulated. It is worth noting that the destruction of ZO-1 causes ZONAB nuclear translocation, which is associated with increased cell proliferation [33]. In addition, ZO-1 and –ZO-2 bind to ZONAB, regulating ZONAB target genes PCNA and cyclin D1 to control cell proliferatio[n] [34]. E-cadherin is also important in cell adhesion-based regulation of cell proliferation. E-cadherin directly binds to β-catenin to regulate cell proliferation via the Wnt signaling pathway [35].

The beneficial effects of realgar in the treatment of NSCLC have been massively investigated in previous studies. For example, Liu et al. evaluated the cytotoxicity of realgar in 4 types of NSCLC cell lines, including H23, A549, H460 and H1650. They demonstrated that realgar could induce apoptosis and inhibit the proliferation of NSCLC cells via inducing ferroptosis by KRAS/Raf/MAPK pathway [36]. Another study revealed that realgar inhibited the viability as well as the glucose consumption of lung cancer stem cells isolated from NSCLC cells [37]. In addition, realgar was proven to suppress the proliferation of other human solid tumor cells, including gastric cancer cell line, malignant melanoma cell line, pancreatic carcinoma cell line and hepatocellular carcinoma cell line. Realgar induces apoptosis and consequently inhibits the tumor cells' activities in a dose- and time-dependent manner [38]. In comparison, our current study was mainly focused on finding the targets of realgar anti-NSCLC. In the present study, we concluded that XO was a possible target of realgar against NSCLC and revealed that XO was a potential marker for the identification and prognosis of patients with NSCLC. However, this study has several limitations. First, although XO is the only key target for a realgar against NSCLC that has been identified, other targets cannot be excluded. Realgar may function on multiple targets and operate in a more complicated manner. In addition, the expression of these two MET markers was detected in this study. Future studies are needed to detect more downstream components of the MET pathway, such as PI3K/AKT and RAS/ERK/MAPK. In addition, the mechanism by which XO regulates the MET signaling pathway remains to be studied in detail. Finally, XO may function in tumor inhibition via other mechanisms, such as autophagy and apoptosis. An in-depth analysis of the anti-NSCLC pharmacological actions of realgar and related targets and pathways requires further verification. Moreover, a large number of experimental validations *in vivo* or *in vitro* are required.

5. Conclusion

In this study, we identified 23 overlapping genes as potential targets of realgar in NSCLC. Enrichment analysis of the GO terms was conducted to determine the possible mechanism of realgar action in NSCLC treatment. TCGA analysis revealed that high expression of *XDH* was associated with poor overall survival in patients with NSCLC, further suggesting XO as a therapeutic target. Molecular docking simulations demonstrated the direct binding potential between realgar and XO. Preliminary *in vitro* experiments were performed to demonstrate the ability of realgar to attenuate XO activity in NSCLC cell lines. Additionally, ROS oxidation, autophagy, and apoptosis are closely associated with *XDH*, indicating the biological significance of XO expression in NSCLC. In conclusion, this study identified XO as a promising target for the treatment of NSCLC and highlighted it as a new therapeutic target for NSCLC.

Funding

This work was supported by the National Natural Science Foundation of China (81900264), Project of Administration of Traditional Chinese Medicine Guangdong Province (20211347), the Shenzhen Science and Technology Innovation Commission (JCYJ20210324130609027 and JCYJ20190814121601671) and the Longgang Medical and Health Science and Technology Project (LGKCYLWS2020040 and LGKCYLWS2019000393).

Ethical approval

Ethical approval was not required for the preparation of this manuscript.

Declaration of competing interest

The authors declare that they have no known competing financial interests or personal relationships that could have appeared to influence the work reported in this paper.

Acknowledgments

We thank Jinbo Lin and Yanqiu Zhao from Central Laboratory, Longgang District People's Hospital of Shenzhen, for their assistance with cellular experiments. We thank Dahai Zeng from the department of IWRM (Institute of Advanced Wear & Corrosion Resistant and Functional Materials) of Jinan University for his help with invaluable discussions.

Appendix A. Supplementary data

Supplementary data related to this article can be found at https://doi.org/10.1016/j.heliyon.2022.e12666.

References

[1] H. Sung, J. Ferlay, R.L. Siegel, et al., Global cancer statistics 2020: GLOBOCAN estimates of incidence and mortality worldwide for 36 cancers in 185 countries, CA Cancer J. Clin. 71 (3) (2021) 209–249, https://doi.org/10.3322/caac.21660.

[2] P. Goldstraw, D. Ball, J.R. Jett, et al., Non-small-cell lung cancer, Lancet 378 (9804) (2011) 1727–1740, https://doi.org/10.1016/S0140-6736(10)62101-0.

[3] H. Lemjabbar-Alaoui, O.U. Hassan, Y.W. Yang, et al., Lung cancer: biology and treatment options, Biochim. Biophys. Acta 1856 (2) (2015) 189–210, https://doi.org/10.1016/j.bbcan.2015.08.002.

[4] H.H. Zhu, J. Hu, F. Lo-Coco, et al., The simpler, the better: oral arsenic for acute promyelocytic leukemia, Blood 134 (7) (2019) 597–605, https://doi.org/10.1182/blood.2019000760.

[5] P. Song, P. Chen, D. Wang, et al., Realgar transforming solution displays anticancer potential against human hepatocellular carcinoma HepG2 cells by inducing ROS, Int. J. Oncol. 50 (2) (2017) 660–670, https://doi.org/10.3892/ijo.2016.3831.

[6] Q.H. Zhao, Y. Zhang, Y. Liu, et al., Anticancer effect of realgar nanoparticles on mouse melanoma skin cancer in vivo via transdermal drug delivery, Med. Oncol. 27 (2) (2010) 203–212, https://doi.org/10.1007/s12032-009-9192-1.

[7] W. Ding, L. Zhang, S. Kim, et al., Arsenic sulfide as a potential anti-cancer drug, Mol. Med. Rep. 11 (2) (2015) 968–974, https://doi.org/10.3892/mmr.2014.2838.

[8] L. Zhang, S. Kim, W. Ding, et al., Arsenic sulfide inhibits cell migration and invasion of gastric cancer in vitro and in vivo, Drug Des. Dev. Ther. 9 (2015) 5579–5590, https://doi.org/10.2147/DDDT.S89805.

[9] W. Ding, T. Ji, W. Xiong, et al., Realgar, a traditional Chinese medicine, induces apoptosis of HPV16-positive cervical cells through a HPV16 E7-related pathway, Drug Des. Dev. Ther. 12 (2018) 3459–3469, https://doi.org/10.2147/DDDT.S172525.

[10] X. Xiaoxia, S. Jing, X. Dongbin, et al., Realgar nanoparticles inhibit migration, invasion and metastasis in a mouse model of breast cancer by suppressing matrix metalloproteinases and angiogenesis, Curr. Drug Delivery 17 (2) (2020) 148–158, https://doi.org/10.2174/1567201817666200115105633.

[11] P. Chen, R. Xu, L. Yan, et al., Properties of realgar bioleaching using an extremely acidophilic bacterium and its antitumor mechanism as an anticancer agent, Biol. Res. 50 (1) (2017) 17, https://doi.org/10.1186/s40659-017-0122-y.

[12] F.R. Yang, Y.F. Zhao, X.W. Hu, et al., Nano-realgar suppresses lung cancer stem cell growth by repressing metabolic reprogramming, Gene 788 (2021), 145666, https://doi.org/10.1016/j.gene.2021.145666.

[13] Y. Yang, J. Yi, J. Chen, et al., Effect of realgar nanoparticles on apoptosis of lung cancer A549 cells, Asia Pac. Tradition. Med. (6) (2010) 14–17 (in Chinese).

[14] Q.F. Yuan, H.J. Li, L.Y. Yu, Effect of nano realgar on expression of vascular endothelial growth factor and hypoxia inducible factor-1 in lung cancer A549 cells, Chin. Gerontol. (3) (2015) 720–722 (in Chinese).

[15] B.G. Kim, H.Y. Kwon, E.J. Sohn, et al., Activation of caspases and inhibition of ribosome biogenesis mediate antitumor activity of Chijongdan in A549 non-small lung cancer cells, BMC Compl. Alternative Med. 14 (2014) 420, https://doi.org/10.1186/1472-6882-14-420.

[16] K. Okamoto, T. Kusano, T. Nishino, Chemical nature and reaction mechanisms of the molybdenum cofactor of xanthine oxidoreductase, Curr. Pharmaceut. Des. 19 (14) (2013) 2606–2614, https://doi.org/10.2174/1381612811319140010.

[17] T. Nishino, K. Okamoto, B.T. Eger, et al., Mammalian xanthine oxidoreductase - mechanism of transition from xanthine dehydrogenase to xanthine oxidase, FEBS J. 275 (13) (2008) 3278–3289, https://doi.org/10.1111/j.1742-4658.2008.06489.x.

[18] N. Kaushik, N. Uddin, G.B. Sim, et al., Responses of solid tumor cells in DMEM to reactive oxygen species generated by non-thermal plasma and chemically induced ROS systems, Sci. Rep. 5 (2015) 8587, https://doi.org/10.1038/srep08587.

[19] H. Xu, C. Li, O. Mozziconacci, et al., Xanthine oxidase-mediated oxidative stress promotes cancer cell-specific apoptosis, Free Radic. Biol. Med. 139 (2019) 70–79, https://doi.org/10.1016/j.freeradbiomed.2019.05.019.

[20] Z. Liu, F. Guo, Y. Wang, et al., BATMAN-TCM: a bioinformatics analysis tool for molecular mechANism of traditional Chinese medicine, Sci. Rep. 6 (2016), 21146, https://doi.org/10.1038/srep21146.

[21] J. Kim, S. So, H.J. Lee, J.C. Park, J.J. Kim, Lee H. DigSee, Disease gene search engine with evidence sentences (version cancer), Nucleic Acids Res. 41 (2013) 510–517, https://doi.org/10.1093/nar/gkt531.

[22] D. Szklarczyk, A.L. Gable, K.C. Nastou, et al., The STRING database in 2021: customizable protein-protein networks, and functional characterization of user-uploaded gene/measurement sets, Nucleic Acids Res. 49 (D1) (2021) D605–D612, https://doi.org/10.1093/nar/gkaa107.

[23] A. Jia, L. Xu, Y. Wang, Venn diagrams in bioinformatics, Briefings Bioinf. 22 (5) (2021) bbab108, https://doi.org/10.1093/bib/bbab108.

[24] B.T. Sherman, da W. Huang, Q. Tan, et al., DAVID Knowledgebase: a gene-centered database integrating heterogeneous gene annotation resources to facilitate high-throughput gene functional analysis, BMC Bioinf. 8 (2007) 426, https://doi.org/10.1186/1471-2105-8-426.

[25] Z. Tang, C. Li, B. Kang, G. Gao, C. Li, Z. Zhang, GEPIA: a web server for cancer and normal gene expression profiling and interactive analyses, Nucleic Acids Res. 45 (2017) 98–102, https://doi.org/10.1093/nar/gkx247.

[26] M. Pathan, S. Keerthikumar, C.S. Ang, et al., FunRich: an open access standalone functional enrichment and interaction network analysis tool, Proteomics 15 (15) (2015) 2597–2601, https://doi.org/10.1002/pmic.201400515.

[27] S. Forli, R. Huey, M.E. Pique, M.F. Sanner, D.S. Goodsell, A.J. Olson, Computational protein-ligand docking and virtual drug screening with the AutoDock suite, Nat. Protoc. 11 (5) (2016) 905–919, https://doi.org/10.1038/nprot.2016.051.

[28] J. Liu, L. Volkers, W. Jangsangthong, et al., Generation and primary characterization of iAM-1, a versatile new line of conditionally immortalized atrial myocytes with preserved cardiomyogenic differentiation capacity, Cardiovasc. Res. 114 (14) (2018) 1848–1859, https://doi.org/10.1093/cvr/cvy134.

[29] P. Naumov, P. Makreski, G. Jovanovski, Direct atomic scale observation of linkage isomerization of As4S4 clusters during the photoinduced transition of realgar to pararealgar, Inorg. Chem. 46 (25) (2007) 10624–10631, https://doi.org/10.1021/ic701299w.

[30] T.T. Luo, Y. Lu, S.K. Yan, et al., Network pharmacology in research of Chinese medicine formula: methodology, application and prospective, Chin. J. Integr. Med. 26 (1) (2020) 72–80, https://doi.org/10.1007/s11655-019-3064-0.

[31] J. Zhu, B. Li, Y. Ji, L. Zhu, Y. Zhu, H. Zhao, β-elemeneelemene inhibits the generation of peritoneum effusion in pancreatic cancer via suppression of the HIF1A-VEGFA pathway based on network pharmacology, Oncol. Rep. 42 (6) (2019) 2561–2571, https://doi.org/10.3892/or.2019.7360.

[32] X.L. Wang, L.I. Yang, D. Liu, et al., Effect of astragalus polysaccharide on autophagy and PI3K/AKT signaling pathway in lung cancer A549 cells induced by xanthine oxidase, Chin. Pharmacol. Bull. 35 (12) (2019) 5 (in Chinese).

[33] M.S. Balda, M.D. Garrett, K. Matter, The ZO-1-associated Y-box factor ZONAB regulates epithelial cell proliferation and cell density, J. Cell Biol. 160 (3) (2003) 423–432, https://doi.org/10.1083/jcb.200210020.

[34] L. Gonzalez-Mariscal, B. Chávez de Ramírez, M. Cereijido, Tight junction formation in cultured epithelial cells (MDCK), J. Membr. Biol. 86 (2) (1985) 113–125, https://doi.org/10.1007/BF01870778.

[35] C.D. Buckley, J. Tan, K.L. Anderson, et al., Cell adhesion. The minimal cadherin-catenin complex binds to actin filaments under force, Science 346 (6209) (2014), 1254211, https://doi.org/10.1126/science.1254211.

[36] X. Liu, Y. Hai, J. Dong, et al., Realgar-induced KRAS mutation lung cancer cell death via KRAS/Raf/MAPK mediates ferroptosis, Int. J. Oncol. 61 (6) (2022) 157, https://doi.org/10.3892/ijo.2022.5447.

[37] F.R. Yang, Y.F. Zhao, X.W. Hu, et al., Nano-realgar suppresses lung cancer stem cell growth by repressing metabolic reprogramming, Gene 788 (2021), 145666, https://doi.org/10.1016/j.gene.2021.145666.

[38] W. Ding, L. Zhang, S. Kim, et al., Arsenic sulfide as a potential anti-cancer drug, Mol. Med. Rep. 11 (2) (2015) 968–974, https://doi.org/10.3892/mmr.2014.2838.